CHAPTER 13

RADIATIVE PROPERTIES OF SEMITRANSPARENT MEDIA

13.1 INTRODUCTION

Any solid or liquid that allows electromagnetic waves to penetrate an appreciable distance into it is known as a semitransparent medium. What constitutes an "appreciable distance" depends, of course, on the physical system at hand. If a thick film on top of a substrate allows a substantial amount of photons to propagate, say, 100 μm into it, the film material would be considered semitransparent. On the other hand, if heat transfer within a large vat of liquid glass is of interest, the glass cannot be considered semitransparent for those wavelengths that cannot penetrate several centimeters through the glass.

Pure solids with perfect crystalline or very regular amorphous structures, as well as pure liquids, gradually absorb radiation as it travels through the medium, but they do not scatter it appreciably within that part of the spectrum that is of interest to the heat transfer engineer. If a solid crystal has defects, or if a solid or liquid contains inclusions (foreign molecules or particles, bubbles, etc.), the material may scatter as well as absorb. In some instances semitransparent media are inhomogeneous and tend to scatter radiation as a result of their inhomogeneities. An example of such material is aerogel [1], a highly transparent, low heat-loss window material made of tiny hollow glass spheres pressed together.

A number of theoretical models exist to predict the absorption and scattering characteristics of semitransparent media. As for opaque surfaces, the applicability of theories is limited, and they must be used in conjunction with experimental data. In this chapter we shall limit ourselves to absorption within semitransparent media. The models describing scattering behavior are the same as the ones presented in the previous chapter and will not be further discussed here. In particular, scattering from turbid media, insulation, foams, etc., has been summarized near the end of Section 12.12.

13.2 ABSORPTION BY SEMITRANSPARENT SOLIDS

The absorption behavior of ionic crystals can be rather successfully modeled by the Lorentz model, which was discussed in some detail in Chapters 2 and 3. The Lorentz theory predicts

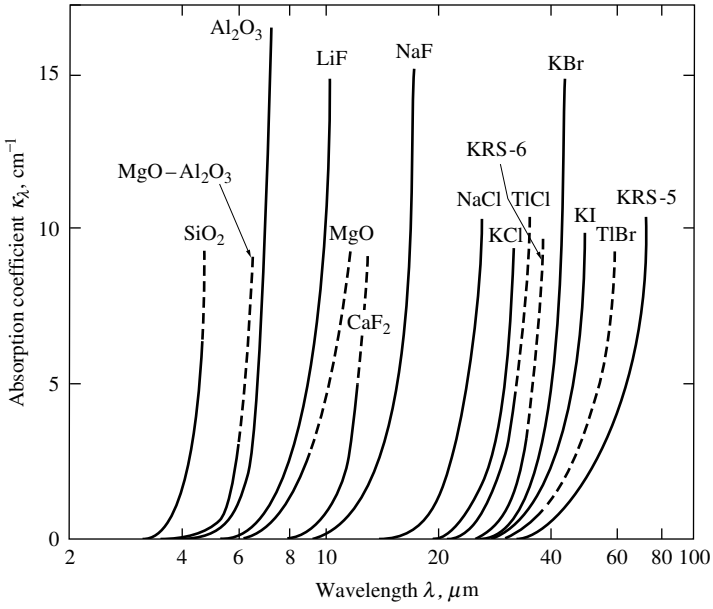

FIGURE 13-1
Spectral absorption coefficients of several ionic crystals at room temperature [2].

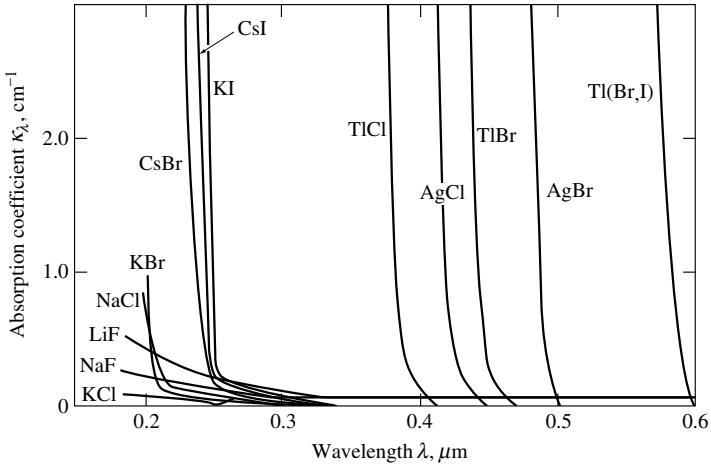

FIGURE 13-2
Spectral absorption coefficient of several halides at room temperature [2].

that an ionic crystal has one or more Reststrahlen bands in the midinfrared ($\lambda > \simeq 5\,\mu$m) (photon excitation of lattice vibrations). The wavelength at which strong absorption commences because of Reststrahlen bands is often called the *long-wavelength absorption edge*. The spectral absorption coefficients and their long-wavelength absorption edges are shown for a number of ionic crystals in Fig. 13-1. Note that these crystals are essentially transparent over much of the near infrared, and become very rapidly opaque at the onset of Reststrahlen bands.

The Lorentz model also predicts that the excitation of valence band electrons, across the band gap into the conduction band, results in several absorption bands at short wavelengths (usually around the ultraviolet). Figure 13-2 shows the absorption coefficient and *short-wavelength absorption edge* for several halides: Materials that are essentially opaque in the ultraviolet become highly transparent in the visible and beyond.

Pure solids are generally highly transparent between the two absorption edges. If large amounts of localized lattice defects and/or dopants (foreign-material molecules called *color centers*) are present, electronic excitations may occur at other wavelengths in between. A number of models predict the absorption characteristics of such defects, some sophisticated, some simple

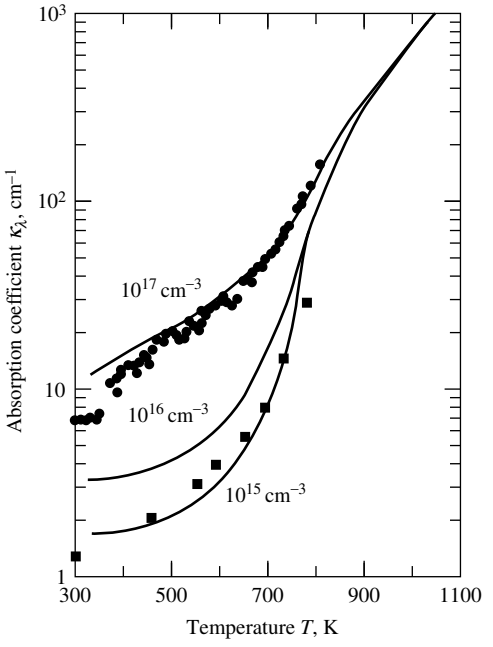

FIGURE 13-3
Spectral absorption coefficient of phosphorus-doped Si at 10.6 μm; solid lines: model of Blomberg and coworkers [4]; square symbols (■): data of Boyd and coworkers [6] (dopant concentration of 1.1×10^{15} cm^{-3}); circular symbols (●): data of Siregar and coworkers [5] (dopant concentration unknown).

and semiempirical. For example, Bhattacharyya and Streetman [3] and Blomberg and coworkers [4] developed models predicting the effect of dopants on the absorption coefficient of silicon. Figure 13-3 shows a comparison of the model by Blomberg and coworkers with experimental data of Siregar and colleagues [5] and Boyd and coworkers [6] for phosphorus-doped silicon at 10.6 μm (a wavelength of great importance for materials processing with CO_2 lasers). The absorption coefficient increases strongly with dopant concentration and with temperature. According to both models, the rise with temperature is due to increases in the number of free electrons and to their individual contributions. The same trends were observed by Timans [7] for the wavelength range between 1.1 and 1.6 μm.

The absorption behavior of amorphous, i.e., noncrystalline solids is much more difficult to predict, although the general trends are quite similar. By far the most important semitransparent amorphous solid is soda–lime glass (ordinary window glass, as opposed to the quartz or silicon dioxide crystals depicted in Fig. 13-1). A number of investigators measured the absorption behavior of window glass, notably Genzel [8], Neuroth [9, 10], Grove and Jellyman [11], and Bagley and coworkers [12]. Figure 1-17 shows the behavior of the spectral absorption coefficient of window glass for a number of different temperatures. As expected from the data for the transmissivity of window panes (Figs. 3-28 and 3-29), glass is fairly transparent for wavelengths $\lambda < 2.5\,\mu$m; beyond that it tends to become rather opaque.

The temperature dependence for quartz has been observed to be similar to that of silicon by Beder and coworkers [13], who reported a fourfold increase of the absorption coefficient between room temperature and 1500°C.

13.3 ABSORPTION BY SEMITRANSPARENT LIQUIDS

The absorption properties of semitransparent liquids are quite similar to those of solids, while they also display some behavior similar to molecular gases. Remnants of intermolecular vibrations (Reststrahlen bands) are observed in many liquids, as are remnants of electronic band gap transitions in the ultraviolet. In the wavelengths in between, molecular vibration bands

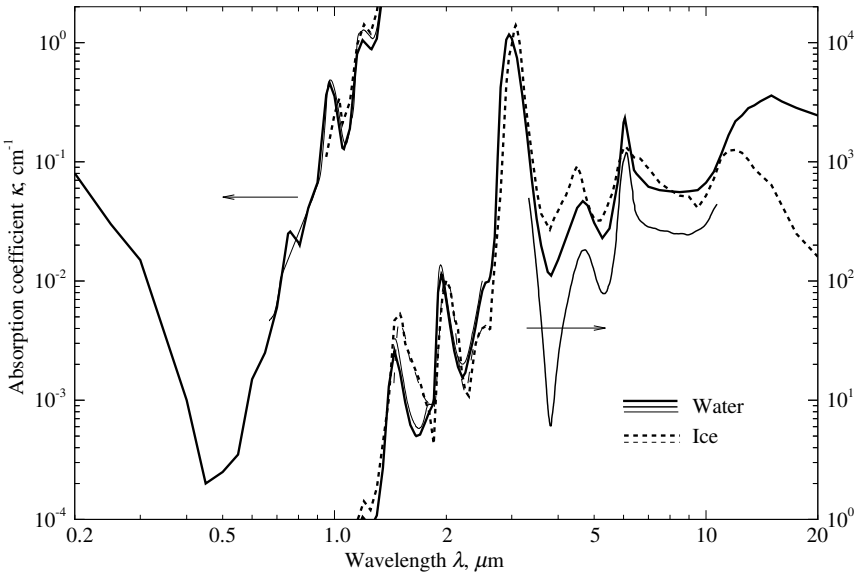

FIGURE 13-4
Spectral absorption coefficient of clear water (at room temperature) and clear ice (at −10°C [14] and −25°C [17]); from [14] (thick lines), [18] (medium line), and [17] (thin lines).

are observed for molecules with permanent dipole moments, similar to the vibration–rotation bands of gases.

Because of its abundance in the world around us (and, indeed, inside our own bodies) the absorption properties of water (and its solid form as ice) are by far the most important and, therefore, have been studied extensively, indeed for centuries. The data of many investigators for clear water and clear ice have been collected and interpreted by Irvine and Pollack [14] and by Ray [15]. Another review, limited to pure water, has been given by Hale and Querry [16]. More recent measurements have been reported by Kou and colleagues [17] (water and ice for wavelengths below 2.5 μm) and by Marley and coworkers [18] (water between 3.3 μm and 11 μm). The spectral absorption coefficient of clear water (at room temperature) and of clear ice (at −10°C) is shown in Fig. 13-4, based on the tabulations of Irvine and Pollack [14], Kou and colleagues [17] and Marley and coworkers [18]. Note the similarity between solid ice and liquid water. The lowest points of the absorption spectra of water and ice lie in the visible, making them virtually transparent over short distances. The minimum point lies in the blue part of the visible ($\lambda \simeq 0.45\,\mu$m): Large bodies of water (or clear ice) transmit blue light the most, giving them a bluish hue. In the near- to midinfrared water and ice display several absorption bands (at 1.45, 1.94, 2.95, 4.7, and 6.05 μm in water, somewhat shifted for ice). These bands are very similar to the water vapor bands at 1.38, 1.87, 2.7, and 6.3 μm (see Table 11.3). Agreement between the data of Irvine and Pollack, and that of Kou and colleagues is excellent, while the data of Marley and coworkers in the longer wavelength region are considerably lower than those of Irvine and Pollack: measurement of such large absorption coefficients is extremely difficult, and the modern measurements of Marley and coworkers list an average estimated error of better than 3%. The temperature dependence of the absorption coefficient of water has been investigated by Goldstein and Penner [19] (up to 209°C) and by Hale and coworkers [20] (up to 70°C) and was found to be fairly weak. As temperature increases, water becomes somewhat more transparent in relatively transparent regions and somewhat more opaque in absorbing regions. A rather detailed discussion of the absorption behavior of clean water and ice has been given by Bohren and Huffman [21]. Natural waters and ice generally contain significant amounts of particulates (small organisms, detritus) and gas bubbles, which tend to increase the absorption rate as well

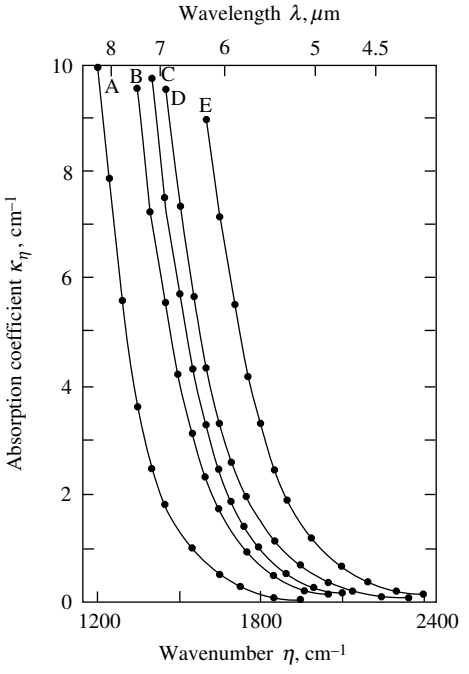

FIGURE 13-5
Spectral absorption coefficient of LiF for various temperatures; A: 300 K; B: 705 K; C: 835 K; D: 975 K; E: 1160 K. The melting point of LiF is 1115 K [22].

as to scatter radiation. While a number of measurements have been made on varieties of natural waters and ice, the results are difficult to correlate since the composition of natural waters varies greatly.

The similarity of absorption behavior between the solid and liquid states of a substance is not limited to water. Barker [22] has measured the absorption coefficient of three alkali halides (KBr, NaCl, and LiF) for several temperatures between 300 K and temperatures above the melting point. Since Reststrahlen bands tend to widen with increasing temperature (see Section 3.5), the long-wavelength absorption edge moves toward shorter wavelengths. No distinct discontinuity in absorption coefficient was observed as the material changed phase from solid to liquid. As an example, the behavior of lithium fluoride (LiF) is depicted in Fig. 13-5. Semiempirical models for the absorption coefficient of alkali halide crystals, resulting in simple formulae, have been given by Skettrup [23] and Woodruff [24], while a similar formula for alkali halide melts has been developed by Senatore and coworkers [25].

13.4 RADIATIVE PROPERTIES OF POROUS SOLIDS

The applicability of the RTE to heterogeneous media was studied by several investigators, e.g., [26–38]. In this section we will assume that heterogeneous media can be modeled as homogeneous with radiative intensity described by a local average value based on appropriate continuum properties.

The radiative properties of open cell carbon foam were studied using experimental techniques and a predictive model by Baillis *et al.* [39]. The model combined elements of geometric optics and diffraction theory applied to the foam geometry determined by microscopic techniques. Extinction, scattering, and absorption coefficients were determined by assuming open cells to consist of struts with varying thickness and strut junctions, as schematically shown in Fig. 13-6, leading to

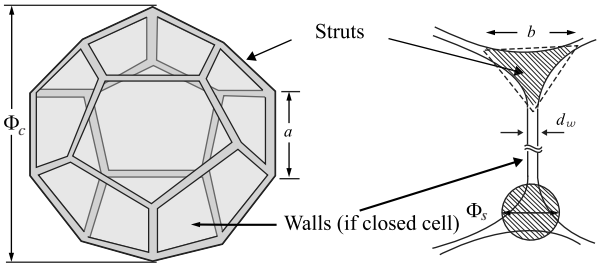

FIGURE 13-6
Schematic of ideal foam cell, consisting of struts (with lengths a and curved triangular cross-section diameter b), strut junctions, and, in the case of closed-cell foams, thin walls of thickness d_w [40].

$$\beta_\lambda = N\left(\bar{G}_1 + \frac{\bar{G}_2}{2}\right), \tag{13.1}$$

$$\sigma_{s\lambda} = \rho_\lambda \beta_\lambda, \tag{13.2}$$

$$\kappa_\lambda = (1 - \rho_\lambda)\beta_\lambda, \tag{13.3}$$

where N is the number of struts per unit volume, $\bar{G}_1$ and $\bar{G}_2$ are the average geometric cross sections of struts and strut junctions, respectively, and ρ_λ is the spectral hemispherical reflectance of the solid.[1] Hemispherical reflectances of foam slabs obtained by solving the RTE with the predicted properties agreed well with measured ones, as shown in Fig. 13-7. Larger discrepancies were observed for the very small, and thus difficult to measure, hemispherical transmittance of a 4.3 mm thick sample.

The radiative properties of highly-porous open-cell metallic foams with inhomogeneities in the size range of geometric optics were studied using simple predictive models by Loretz *et al.* [42]. The foam structure was determined using microscopic and tomographic techniques. The cells (Fig. 13-6) were assumed to consist of struts and strut junctions. The extinction coefficient of the cells modeled as pentagon dodecahedrons or tetracaedecahedrons was obtained using the Glicksman and Torpey model [43]:

$$\beta = 4.09\sqrt{\frac{1-\varepsilon}{D^2}}, \tag{13.4}$$

where ε and D are the porosity and average cell diameter, respectively. For pentagon dodecahedrons with neglected strut junctions equation (13.4) becomes

$$\beta = \frac{3}{4}1.305\frac{b}{a^2}, \tag{13.5}$$

[1]The factor of $\frac{1}{2}$ in equation (13.1) is not present in the original paper [39], but was added in more recent work, e.g., [41], perhaps to account for the fact that foam contains fewer strut junctions than struts.

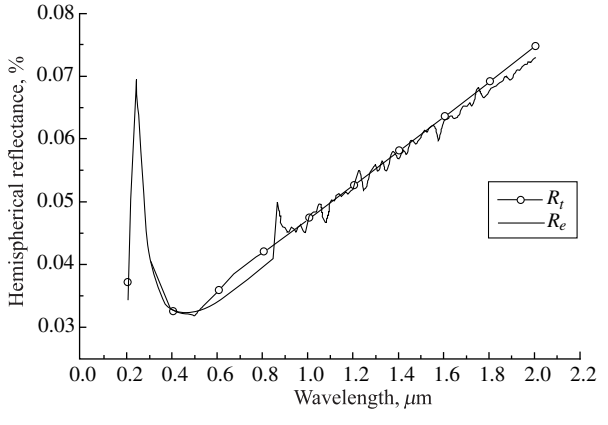

FIGURE 13-7
Hemispherical reflectance for carbon foam sample 4.3 mm thick for normal incidence; experimental (R_e) and theoretical (R_t) results [39].

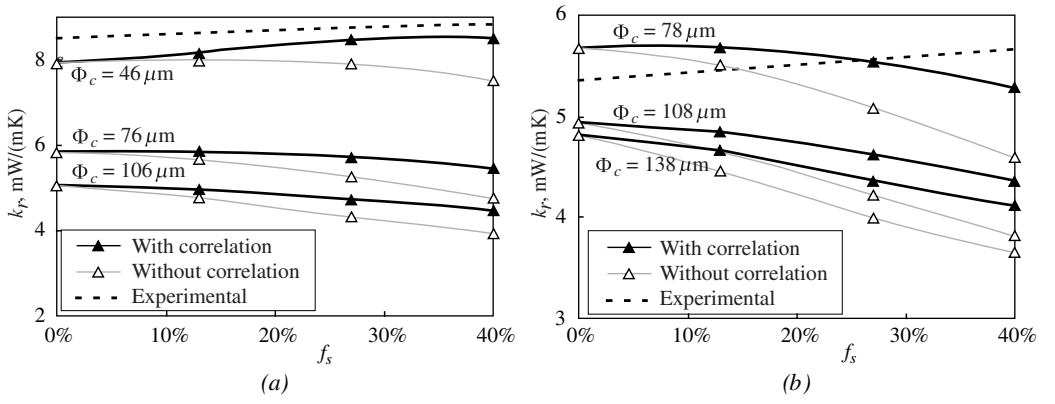

FIGURE 13-8
Radiative conductivity for two different extruded polystyrene foams [40]. Φ_c is the diameter of the foam cell measured as *(a)* $\Phi_c = 76 \pm 30\,\mu$m and *(b)* $\Phi_c = 108 \pm 30\,\mu$m, respectively. Both predicted and "measured" conductivities depend on the unknown solid fraction contained in struts, f_s.

where a and b are the strut length and average thickness, respectively, as indicated in Fig. 13-6.

The radiative properties of closed-cell foams were studied for expanded polystyrene foam by Coquard *et al.* [44,45], and those for extruded polystyrene foams were predicted and verified experimentally by Kaemmerlen and coworkers [40]. The properties were determined using the integration method of [46] applied to the curved-triangular foam cell wall and strut geometries of Fig. 13-6. Radiative conductivity k_r was calculated employing the Rosseland-mean extinction coefficient, which in turn was calculated by independently determining the extinction coefficients of struts and of thin films of polystyrene. Due to the low density of the foam, independent scattering was assumed to hold, and the bulk extinction coefficient was determined by adding contributions from struts and walls, similar to equation (13.1). Figure 13-8 shows k_r with and without a correction factor to the scattering efficiency to account for the concave shape of circular struts, which leads to a noticeable decrease in the variation of k_r with the strut fraction as compared to the uncorrected results. However, as the authors noticed, the trends between predicted and measured radiative conductivities are different.

A more extensive discussion of the radiative properties of open-cell and closed-cell foams may be found in the book by Dombrovsky and Baillis [41].

Monte Carlo ray tracing methods have been employed in a number of studies for the determination of effective radiative properties of heterogeneous media based on the geometry and properties of individual medium components. Tancrez and Taine [29] presented methodology for porous media with opaque solid phase, which was extended to media with semitransparent solids [33]. Coquard and Baillis applied ray tracing to determine the radiative properties of beds of opaque, diffusely or specularly reflecting particles [47]. The latter study was extended to beds of spheres containing an absorbing and scattering medium [48], and also applied to the actual geometry of polymeric foams obtained by tomography [49]. Also using tomography, the geometry of reticulated porous ceramics (RPC) with an opaque solid phase was obtained by Petrasch *et al.* [50] and by Haussener *et al.* [51]; the latter also used this technique for reacting packed beds with an opaque solid phase [52]. Finally, mullite foam with a semitransparent solid phase was studied by Zeghondy and coworkers [33]. In the tomography-based Monte Carlo methods used to study radiative properties of reticulated porous ceramics (Fig. 13-9) [29, 33, 50, 51] the media were assumed to be statistically homogeneous and isotropic, and the solid phase was assumed to be opaque. Diffraction effects were neglected and geometric optics was assumed to be valid. A large number N_r of stochastic rays were launched in the void phase of a subvolume V_0 of a representative elementary volume V. Rays were traced until they interacted with the solid–void interface or were lost at the faces of V. For each ray colliding with the solid phase the

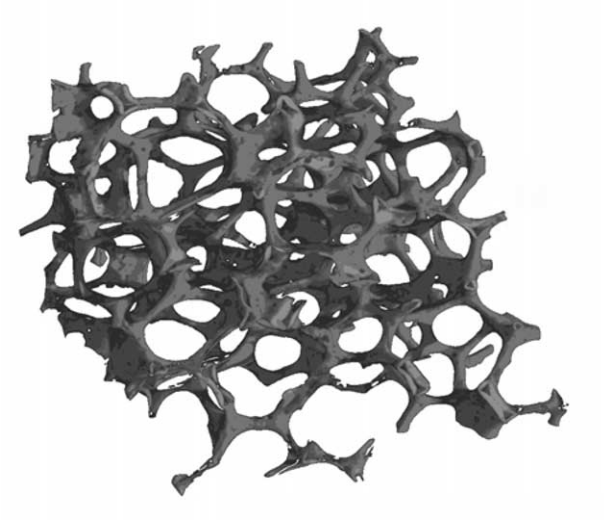

FIGURE 13-9
3D rendering of Rh-coated reticulated porous ceramics with nominal pore diameter d_{nom} = 2.54 mm obtained using computed tomography techniques [50].

distance to collision was recorded, and rays were either absorbed or reflected, either specularly or diffusely. The distribution function for attenuation path length was then computed as

$$F_s = \frac{1}{N_r} \int_{s^*=0}^{s} dN(s) = 1 - \exp(-\beta s), \tag{13.6}$$

where $dN(s)$ is the number of rays attenuated within ds around s; F_s quantifies the probability of a ray hitting the solid–void interface at a location between 0 and s. The scattering and absorption coefficients were then obtained from equations (13.2) and (13.3).

Figure 13-10 shows the radiative intensity obtained numerically and experimentally as a function of normalized path length. The relative difference of 10% between experimental (β_{ex}) and Monte Carlo-determined (β_{MC}) extinction coefficient was attributed to the effect of local material anisotropy for finite and relatively small RPC samples. Monte Carlo results were integrated over all solid angles, while the experimental measurements were carried out only along a single direction.

13.5 EXPERIMENTAL METHODS

The spectral absorption coefficient of a semitransparent solid or liquid can be measured in several ways. The simplest and most common method is to measure the transmissivity of a sample of known thickness, as described in Section 12.12 for particulate clouds. Since solids and liquids reflect energy at the air interfaces, the transmissivity is often determined by forming a ratio between the transmitted signals from two samples of different thickness. However, the transmission method is not capable of measuring very small or very large absorption coefficients: For samples with large transmissivity small errors in the determination of transmissivity, τ, lead to very large errors for the absorption coefficient, κ (since κ is proportional to $\ln \tau$). On the other hand, for a material with large κ sufficient energy for transmission measurements can be passed only through extremely thin samples. Such samples are usually prepared as vacuum-deposited thin films, which do not have the same properties as the parent material [54].

The absorption coefficient may also be determined through a number of different reflection techniques. The reflectivity of an optically smooth interface of a semitransparent medium depends, through the complex index of refraction, on the refractive index n as well as the absorptive index k. In turn, k is related to the absorption coefficient through equation (3.79) as $\kappa = 4\pi\eta k/n$, where $\eta = 1/\lambda$ is the wavenumber of the radiation inside the medium. Thus,

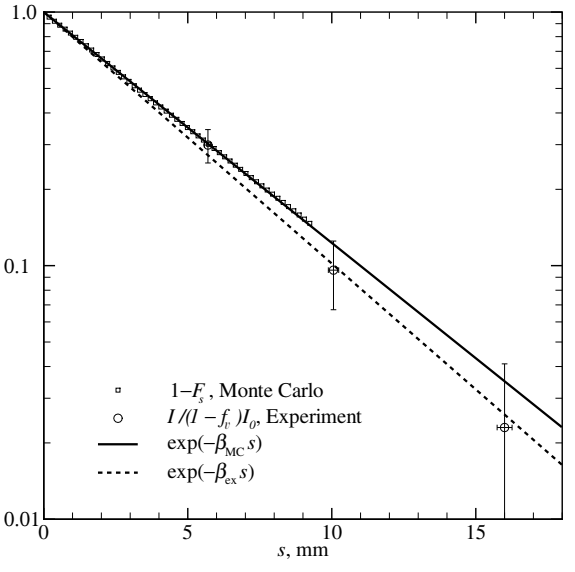

FIGURE 13-10
Variation of radiative intensity in Rh-coated reticulated porous ceramics obtained numerically (squares) and experimentally (circles) as a function of the normalized path length, along with exponential fits with $\beta_{MC} = 210\,m^{-1}$ and $\beta_{ex} = 230\,m^{-1}$ [53].

two data points are necessary to determine n and k. Noting the directional dependence of reflectivity on $m = n - ik$, some researchers have measured the specular reflectivity at two different angles. Leupacher and Penzkofer [55] showed that this can lead to very substantial errors. Other researchers have measured the reflectivity at a single angle, using parallel- and perpendicular-polarized light (known as an *ellipsometric technique*). However, this may also lead to large errors [55]. A new method overcoming these problems has been proposed by Lu and Penzkofer [56]. Using parallel-polarized light they vary the incidence angle until the point of minimum reflectivity at Brewster's angle is found (cf. Figs. 2-8 and 2-11).

Another reflection technique exploits the fact that a *causal relationship* exists between n and k, i.e., they are not independent of one another. This causal relationship is known as the *Kramers–Kronig relation*, which may be expressed as

$$\delta(\eta) = \frac{\eta}{\pi} \int_0^\infty \frac{\ln \rho_n(\eta')}{\eta^2 - \eta'^2}\, d\eta', \tag{13.7}$$

where $\rho_n(\eta)$ is the spectral, normal reflectivity of the sample surface [cf. equation (2.114)], and $\delta(\eta)$ is the phase angle of the complex reflection coefficient, equation (2.111),

$$\widetilde{r}_n = \sqrt{\rho_n}\, e^{i\delta} = \frac{n - ik - 1}{n - ik + 1}. \tag{13.8}$$

Thus, if ρ_n is measured for a large part of the spectrum, the phase angle δ may be determined from equation (13.7) for wavenumbers well inside the measured spectrum; n and k are then readily found from equation (13.8). The method is particularly well suited to experiments employing an FTIR (Fourier transform infrared) spectrometer, which can take broad spectrum measurements over very short times, and which often have a built-in Kramers–Kronig analysis capability. More detailed discussions on the various Kramers–Kronig relations may be found, for example, in the books by Wooten [57] and Bohren and Huffman [21]. A description of the numerical evaluation of equation (13.7) has been given by Wooten [57].

Measurement of physical properties at high temperatures is always difficult, but particularly so for semitransparent media since *two* properties need to be measured (absorption coefficient as well as interface reflectivity, or equivalently, n and k). Myers and coworkers [58] have given a good review of such methods for solid samples. They also developed a new method

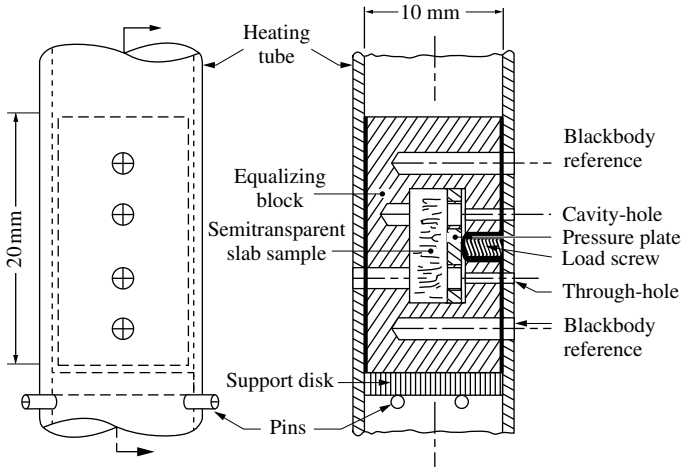

FIGURE 13-11
Sample and holder, mounted within heating tube, for device to determine the optical properties of small, semitransparent solid samples [58].

to determine the optical properties of small, semitransparent, solid samples. Their device is essentially a compact arrangement of that employed by Stierwalt [59], which takes three different radiance measurements in rapid succession. A front and cross-sectional view of their sample heating arrangement is shown in Fig. 13-11. The slab-shaped sample is mounted within an equalizing nickel block, which is coupled radiatively to the electrically heated tube. The nickel block has four cavities and holes serving as radiance targets. A water-cooled graphite block (not shown) is positioned behind the heating tube to provide a room-temperature background for the through-hole as well as a reference for the detector. Three radiance measurements are made and compared with the reference: (*i*) the slab sample positioned in front of the blackbody (cavity-hole), (*ii*) the freely radiating sample (through-hole), and (*iii*) the blackbody reference. With the relations given in Section 3.8 one can use these measurements to deduce the optical properties (n, k, and κ). The method has the advantages that measurements at high temperatures ($\simeq$ 1000°C) can be taken, that only a single sample is necessary, and that no optically smooth surfaces are required. On the other hand, the method suffers from the standard weaknesses of transmission methods (see discussion at the beginning of this section), and is restricted to high temperatures (to produce a strong enough emission signal).

Measurements of the optical properties of a high-temperature liquid are even more challenging. It is more difficult to confine a liquid in a sample holder (which must be horizontal), and more difficult to measure the thickness of the liquid layer. In addition, the layer thickness may be nonuniform because of (often unknown) surface tension effects. Furthermore, high-temperature liquids are often highly reactive, making a sealed chamber necessary. If the vapor pressure becomes substantial at high temperatures, the windows of the sealed chamber will be attacked. Shvarev and coworkers [60] have measured the optical properties of liquid silicon in the wavelength range of 0.4–1.0 μm with such a sealed-chamber furnace apparatus, using an ellipsometric technique. Barker [22, 61] designed an apparatus to measure the optical properties of semitransparent solid slabs and corrosive melts. To isolate the specimen he relied on a windowless chamber with continuous inert-gas purging. His data evaluation required independent measurements of the interface reflectivity, the reflectivity of a platinum mirror, the sample overall reflectivity, and the thickness of the sample. In addition, the reflectivity of the platinum–liquid interface must be estimated. As such, Barker's method appears to be very vulnerable to experimental error.

A more accurate device, limited to absorption coefficients of liquids, has been reported by Ebert and Self [62]. A schematic of their apparatus is shown in Fig. 13-12*a*. The aperture of a blackbody source at 1700°C is imaged (by the spherical mirror M3) onto the platinum mirror located in an alumina crucible inside the furnace. The reflected signal is focused onto

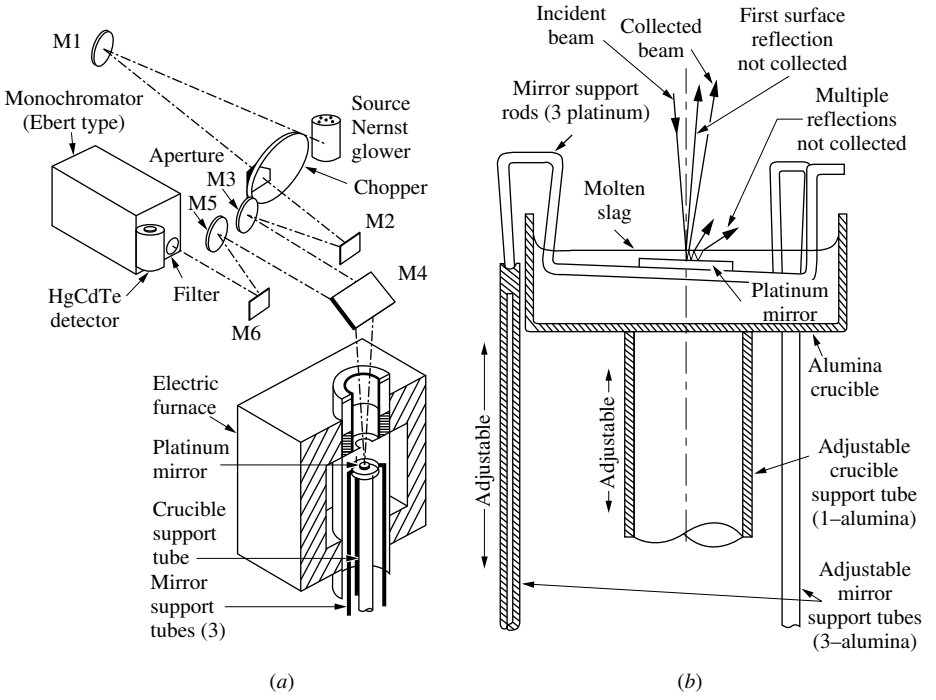

FIGURE 13-12
Measurement of absorption coefficients of high-temperature liquids. (*a*) Schematic of apparatus of Ebert and Self [62], (*b*) schematic of their submerged reflector arrangement.

the monochromator and detector via another spherical mirror (M5). The beam is chopped to eliminate emission as well as background radiation from the signal. The transmissivity of the liquid is measured by what they called a "submerged reflector method," illustrated in Fig. 13-12*b*: A platinum mirror, which may be adjusted via three support rods, is submerged below the surface of the liquid filling the crucible. The platinum mirror is tilted slightly from the horizontal to allow the first surface reflection and multiple internal reflections to be rejected from the collection optics. The thickness of the liquid layer is adjusted by raising and lowering the crucible (leaving the platinum mirror in place). As in the transmission technique, signals for two different layer thicknesses (d_1 and d_2) are ratioed, giving the transmissivity for a layer of thickness $2\,(d_2 - d_1)$. By rejecting the first reflection, and by being able to produce and measure very thin liquid layers, they were able to measure absorption coefficients an order of magnitude higher than Barker, reporting values as high as $70\,\text{cm}^{-1}$ for synthetic molten slags [62]. Similar measurements have been carried out by Gupta and Modest [63] (lithium salts), by Makino and coworkers [64] (alkali metal carbonates), and by Zhang and colleagues [65] (liquid glasses).

Foams and Packed Fibers. Measurements on foams were done by Kuhn and coworkers [66] (polystyrene and polyurethane foam insulation), Sacadura *et al.* [67–69] (fiberglass and carbon foam), Mital and colleagues [70], and Hendricks and Howell [71] (reticulated porous ceramics). The bidirectional reflectance of mullite foam has been measured by Zeghondy and coworkers [72], which agreed well with model results based on the Monte Carlo tool of Tancrez and Taine [29, 33]. Cunnington and coworkers [73] measured the scattering from individual, coated silica fibers, and found qualitative agreement with a theoretical model. Cunnington and Lee measured direct transmissivity and hemispherical reflectivity of randomly packed, high-porosity fibrous material (tiles from the Space Shuttle) [74], and for aerogel-reinforced fibrous material [75]; comparison with Lee's models [76–79] showed excellent agreement for both materials.

References

1. Caps, R., and J. Fricke: "Infrared radiative heat transfer in highly transparent silica aerogel," *Solar Energy*, vol. 36, no. 4, pp. 361–364, 1986.
2. Smakula, A.: "Synthetic crystals and polarizing materials," *Optica Acta*, vol. 9, pp. 205–222, 1962.
3. Bhattacharyya, A., and B. G. Streetman: "Theoretical considerations regarding pulsed CO_2 laser annealing of silicon," *Solid State Communications*, vol. 36, pp. 671–675, 1980.
4. Blomberg, M., K. Naukkarinen, T. Tuomi, V. M. Airaksinen, M. Luomajarvi, and E. Rauhala: "Substrate heating effects in CO_2 laser annealing of ion-implanted silicon," *Journal of Applied Physics*, vol. 54, no. 5, pp. 2327–2328, 1983.
5. Siregar, M. R. T., W. Lüthy, and K. Affolter: "Dynamics of CO_2 laser heating in the processing of silicon," *Applied Physics Letters*, vol. 36, pp. 787–788, 1980.
6. Boyd, I. W., J. I. Binnie, B. Wilson, and M. J. Colles: "Absorption of infrared radiation in silicon," *Journal of Applied Physics*, vol. 55, no. 8, pp. 3061–3063, 1984.
7. Timans, P. J.: "Emissivity of silicon at elevated temperatures," *Journal of Applied Physics*, vol. 74, no. 10, pp. 6353–6364, 1993.
8. Genzel, L.: "Messung der Ultrarot-Absorption von Glas zwischen 20°C and 1360°C (measurement of infrared absorption of glass between 20°C and 1360°C)," *Glastechnische Berichte*, vol. 24, no. 3, pp. 55–63, 1951.
9. Neuroth, N.: "Der Einfluss der Temperatur auf die spektrale Absorption von Gläsern im Ultraroten, I (Effect of temperature on spectral absorption of glasses in the infrared, I)," *Glastechnische Berichte*, vol. 25, pp. 242–249, 1952.
10. Neuroth, N.: "Der Einfluss der Temperatur auf die spektrale Absorption von Gläsern im Ultraroten, II (Effect of temperature on spectral absorption of glasses in the infrared, II)," *Glastechnische Berichte*, vol. 26, pp. 66–69, 1953.
11. Grove, F. J., and P. E. Jellyman: "The infrared transmission of glass in the range from room temperature to 1400°C," *Journal of the Society of Glass Technology*, vol. 39, no. 186, pp. 3–15, 1955.
12. Bagley, B. G., E. M. Vogel, W. G. French, G. A. Pasteur, J. N. Gan, and J. Tauc: "The optical properties of soda-lime-silica glass in the region from 0.006 to 22 eV," *Journal of Non-Crystalline Solids*, vol. 22, pp. 423–436, 1976.
13. Beder, E. C., C. D. Bass, and W. L. Shackleford: "Transmissivity and absorption of fused quartz between 0.2 μm and 3.5 μm from room temperature to 1500°C," *Applied Optics*, vol. 10, pp. 2263–2268, 1971.
14. Irvine, W. M., and J. B. Pollack: "Infrared optical properties of water and ice spheres," *ICARUS*, vol. 8, pp. 324–360, 1968.
15. Ray, P. S.: "Broadband complex refractive indices of ice and water," *Applied Optics*, vol. 11, pp. 1836–1844, 1972.
16. Hale, G. M., and M. R. Querry: "Optical constants of water in the 200 nm to 200 μm wavelength region," *Applied Optics*, vol. 12, pp. 555–563, 1973.
17. Kou, L., D. Labrie, and P. Chylek: "Refractive indices of water and ice in the 0.65 to 2.5 μm spectral range," *Applied Optics*, vol. 32, pp. 3531–3540, 1993.
18. Marley, N. A., J. S. Gaffney, and M. M. Cunningham: "Lambert absorption coefficients of water in the frequency range of 3000–934 cm^{-1}," *Applied Optics*, vol. 33, pp. 8041–8054, 1994.
19. Goldstein, R. J., and S. S. Penner: "The near-infrared absorption of liquid water at temperatures between 27 and 209°C," *Journal of Quantitative Spectroscopy and Radiative Transfer*, vol. 4, pp. 441–451, 1964.
20. Hale, G. M., M. R. Querry, A. N. Rusk, and D. Williams: "Influence of temperature on the spectrum of water," *Journal of the Optical Society of America*, vol. 62, pp. 1103–1108, 1972.
21. Bohren, C. F., and D. R. Huffman: *Absorption and Scattering of Light by Small Particles*, John Wiley & Sons, New York, 1983.
22. Barker, A. J.: "The effect of melting on the multiphonon infrared absorption spectra of KBr, NaCl, and LiF," *Journal of Physics C: Solid State Physics*, vol. 5, pp. 2276–2282, 1972.
23. Skettrup, T.: "Urbach's rule and phase fluctuations of the transmitted light," *Physica Status Solidi (b)*, vol. 103, pp. 613–621, 1981.
24. Woodruff, T. O.: "Empirically derived formula for the energies of the first ultraviolet absorption maximum of 20 alkali-halide crystals," *Solid State Communications*, vol. 46, pp. 139–142, 1983.
25. Senatore, G., M. P. Tosi, and T. O. Woodruff: "A simple formula for the fundamental optical absorption of alkali halide melts," *Solid State Communications*, vol. 52, no. 2, pp. 173–176, 1984.
26. Singh, B. P., and M. Kaviany: "Radiative transfer in packed and fluidized beds: Dependent versus independent scattering," *International Journal of Heat and Mass Transfer*, vol. 34, pp. 2869–2882, 1991.
27. Singh, B. P., and M. Kaviany: "Modelling radiative heat transfer in packed beds," *International Journal of Heat and Mass Transfer*, vol. 35, pp. 1397–1405, 1992.
28. Consalvi, J., B. Porterie, and J. Loraud: "A formal averaging procedure for radiation heat transfer in particulate media," *International Journal of Heat and Mass Transfer*, vol. 45, pp. 2755–2768, 2002.
29. Tancrez, M., and J. Taine: "Direct identification of absorption and scattering coefficients and phase function of a porous medium by a Monte Carlo technique," *International Journal of Heat and Mass Transfer*, vol. 47, pp. 373–383, 2004.
30. Taine, J., and E. Iacona: "Upscaling statistical methodology for radiative transfer in porous media: New trends," *ASME Journal of Heat Transfer*, vol. 134, p. 031012, 2012.

31. Baillis, D., and J.-F. Sacadura: "Thermal radiation properties of dispersed media: Theoretical prediction and experimental characterization," *Journal of Quantitative Spectroscopy and Radiative Transfer*, vol. 67, pp. 327–363, 2000.
32. Coquard, R., D. Baillis, and J. Randrianalisoa: "Homogeneous phase and multi-phase approaches for modeling radiative transfer in foams," *International Journal of Thermal Sciences*, vol. 50, pp. 1648–1663, 2011.
33. Zeghondy, B., E. Iacona, and J. Taine: "Determination of the anisotropic radiative properties of a porous material by radiative distribution function identification (RDFI)," *International Journal of Heat and Mass Transfer*, vol. 49, pp. 2810–2819, 2006.
34. Gusarov, A. V.: "Homogenization of radiation transfer in two-phase media with irregular phase boundaries," *Physical Review B*, vol. 77, pp. 144201–1–14, 2008.
35. Gusarov, A. V.: "Model of radiative heat transfer in heterogeneous multiphase media," *Physical Review B*, vol. 81, p. 064202, 2010.
36. Lipiński, W., J. Petrasch, and S. Haussener: "Application of the spatial averaging theorem to radiative heat transfer in two-phase media," *Journal of Quantitative Spectroscopy and Radiative Transfer*, vol. 111, no. 1, pp. 253–258, 2010.
37. Lipiński, W., D. Keene, S. Haussener, and J. Petrasch: "Continuum radiative heat transfer modeling in media consisting of optically distinct components in the limit of geometrical optics," *Journal of Quantitative Spectroscopy and Radiative Transfer*, vol. 111, no. 16, pp. 2474–2480, 2010.
38. Petrasch, J., S. Haussener, and W. Lipiński: "Application of the spatial averaging theorem to radiative heat transfer in two-phase media," *Journal of Quantitative Spectroscopy and Radiative Transfer*, vol. 112, pp. 1450–1459, 2011.
39. Baillis, D., M. Raynaud, and J.-F. Sacadura: "Determination of spectral radiative properties of open cell foam: Model validation," *Journal of Thermophysics and Heat Transfer*, vol. 14, no. 2, pp. 137–143, 2000.
40. Kaemmerlen, A., C. Vo, F. Asllanaj, G. Jeandel, and D. Baillis: "Radiative properties of extruded polystyrene foams: Predictive model and experimental results," *Journal of Quantitative Spectroscopy and Radiative Transfer*, vol. 111, pp. 865–877, 2010.
41. Dombrovsky, L. A., and D. Baillis: *Thermal Radiation in Disperse Systems: An Engineering Approach*, Begell House, New York, 2010.
42. Loretz, M., R. Coquard, D. Baillis, and E. Maire: "Metallic foams: Radiative properties/comparison between different models," *Journal of Quantitative Spectroscopy and Radiative Transfer*, vol. 109(1), pp. 16–27, 2008.
43. Glicksman, L. R., and M. Torpey: "A study of radiative heat transfer through foam insulation," Technical report, Massachusetts Institute of Technology, Cambridge, MA, 1988.
44. Coquard, R., and D. Baillis: "Modeling of heat transfer in low-density EPS foams," *ASME Journal of Heat Transfer*, vol. 128, pp. 538–549, 2006.
45. Coquard, R., D. Baillis, and D. Quenard: "Radiative properties of expanded polystyrene foams," *ASME Journal of Heat Transfer*, vol. 131, p. 012702, 2009.
46. Placido, E., M. C. Arduini-Schuster, and J. Kuhn: "Thermal properties predictive model for insulating foams," *Infrared Physics and Technology*, vol. 46, pp. 219–231, 2005.
47. Coquard, R., and D. Baillis: "Radiative characteristics of opaque spherical particle beds: A new method of prediction," *Journal of Thermophysics and Heat Transfer*, vol. 18, pp. 178–186, 2004.
48. Coquard, R., and D. Baillis: "Radiative characteristics of beds of spheres containing an absorbing and scattering medium," *Journal of Thermophysics and Heat Transfer*, vol. 19, pp. 226–234, 2005.
49. Coquard, R., D. Baillis, and E. Maire: "Numerical investigation of the radiative properties of polymeric foams from tomographic images," *Journal of Thermophysics and Heat Transfer*, vol. 24, pp. 647–658, 2010.
50. Petrasch, J., P. Wyss, and A. Steinfeld: "Tomography-based Monte Carlo determination of radiative properties of reticulate porous ceramics," *Journal of Quantitative Spectroscopy and Radiative Transfer*, vol. 105, no. 2, pp. 180–197, 2007.
51. Haussener, S., P. Coray, W. Lipiński, P. Wyss, and A. Steinfeld: "Tomography-based heat and mass transfer characterization of reticulate porous ceramics for high-temperature processing," *ASME Journal of Heat Transfer*, vol. 132, p. 023305, 2010.
52. Haussener, S., W. Lipiński, P. Wyss, and A. Steinfeld: "Tomography-based analysis of radiative transfer in reacting packed beds undergoing a solid-gas thermochemical transformation," *ASME Journal of Heat Transfer*, vol. 132, p. 061201, 2010.
53. Coray, P., J. Petrasch, W. Lipiński, and A. Steinfeld: "Determination of radiative characteristics of reticulate porous ceramics," in *Proceedings of the ICHMT Fifth International Symposium on Radiative Transfer*, eds. M. P. Mengüç and N. Selçuk, Bodrum, Turkey, 2007.
54. Viskanta, R., and E. E. Anderson: "Heat transfer in semi-transparent solids," in *Advances in Heat Transfer*, vol. 11, Academic Press, New York, pp. 317–441, 1975.
55. Leupacher, W., and A. Penzkofer: "Refractive-index measurement of absorbing condensed media," *Applied Optics*, vol. 23, no. 10, pp. 1554–1558, 1984.
56. Lu, Y., and A. Penzkofer: "Optical constants measurements of strongly absorbing media," *Applied Optics*, vol. 25, no. 1, pp. 221–225, 1986.
57. Wooten, F.: *Optical Properties of Solids*, Academic Press, New York, 1972.
58. Myers, V. H., A. Ono, and D. P. DeWitt: "A method for measuring optical properties of semitransparent materials at high temperatures," *AIAA Journal*, vol. 24, no. 2, pp. 321–326, 1986.

59. Stierwalt, D. L.: "Infrared spectral emittance of optical materials," *Applied Optics*, vol. 5, no. 12, pp. 1911–1915, 1966.
60. Shvarev, K. M., B. A. Baum, and P. V. Gel'd: "Optical properties of liquid silicon," *Sov. Phys. Solid State*, vol. 16, no. 11, pp. 2111–2112, May 1975.
61. Barker, A. J.: "A compact, windowless reflectance furnace for infrared studies of corrosive melts," *Journal of Physics E: Scientific Instruments*, vol. 6, pp. 241–244, 1973.
62. Ebert, J. L., and S. A. Self: "The optical properties of molten coal slag," in *Heat Transfer Phenomena in Radiation, Combustion and Fires*, vol. HTD-106, ASME, pp. 123–126, 1989.
63. Gupta, S. B., and M. F. Modest: "Measurement of infrared absorption coefficient of molten LiF and Li_2S," *28th AIAA Thermophysics Conference, Orlando, Florida,* AIAA paper no. 93-2760, 1993.
64. Makino, T., M. Edamura, A. Kato, and A. Yoshida: "Thermal radiation properties of molten salt (properties of alkali metal carbonates)," *Heat Transfer – Japanese Research*, vol. 21, no. 4, pp. 331–339, 1992.
65. Zhang, Z., M. F. Modest, and S. P. Bharadwaj: "Measurement of infrared absorption coefficients of molten glasses," *Experimental Heat Transfer*, vol. 14, no. 3, pp. 145–156, 2001.
66. Kuhn, J., H. P. Ebert, M. C. Arduini-Schuster, D. Buettner, and J. Fricke: "Thermal transport in polystyrene and polyurethane foam insulations," *International Journal of Heat and Mass Transfer*, vol. 35, no. 7, pp. 1795–1801, 1992.
67. Nicolau, V. P., M. Raynaud, and J.-F. Sacadura: "Spectral radiative properties identification of fiber insulating materials," *International Journal of Heat and Mass Transfer*, vol. 37, pp. 311–324, 1994.
68. Doermann, D., and J.-F. Sacadura: "Heat transfer in open cell foam insulation," *ASME Journal of Heat Transfer*, vol. 118, no. 1, pp. 88–93, 1996.
69. Baillis, D., M. Raynaud, and J.-F. Sacadura: "Spectral radiative properties of open-cell foam insulation," *Journal of Thermophysics and Heat Transfer*, vol. 13, no. 3, pp. 292–298, 1999.
70. Mital, R., J. P. Gore, and R. Viskanta: "Measurements of radiative properties of cellular ceramics at high temperatures," *Journal of Thermophysics and Heat Transfer*, vol. 10, no. 1, pp. 33–38, January-March 1996.
71. Hendricks, T. J., and J. R. Howell: "Absorption/scattering coefficients and scattering phase functions in reticulated porous ceramics," *ASME Journal of Heat Transfer*, vol. 118, no. 1, pp. 79–87, 1996.
72. Zeghondy, B., E. Iacona, and J. Taine: "Experimental and RDFI calculated radiative properties of a mullite foam," *International Journal of Heat and Mass Transfer*, vol. 49, pp. 3702–3707, 2006.
73. Cunnington, G. R., T. W. Tong, and P. S. Swathi: "Angular scattering of radiation from coated cylindrical fibers," *Journal of Quantitative Spectroscopy and Radiative Transfer*, vol. 48, no. 4, pp. 353–362, 1992.
74. Cunnington, G. R., and S. C. Lee: "Radiative properties of fibrous insulations: Theory versus experiments," *Journal of Thermophysics and Heat Transfer*, vol. 10, no. 3, pp. 460–466, 1996.
75. Cunnington, G. R., S. C. Lee, and S. M. White: "Radiative properties of fiber-reinforced aerogel: Theory versus experiment," *Journal of Thermophysics and Heat Transfer*, vol. 12, no. 1, pp. 17–22, 1998.
76. Lee, S. C.: "Radiative transfer through a fibrous medium: Allowance for fiber orientation," *Journal of Quantitative Spectroscopy and Radiative Transfer*, vol. 36, no. 3, pp. 253–263, 1986.
77. Lee, S. C.: "Radiation heat-transfer model for fibers oriented parallel to diffuse boundaries," *Journal of Thermophysics and Heat Transfer*, vol. 2, no. 4, pp. 303–308, Oct 1988.
78. Lee, S. C.: "Effect of fiber orientation on thermal radiation in fibrous media," *International Journal of Heat and Mass Transfer*, vol. 32, no. 2, pp. 311–320, 1989.
79. Lee, S. C.: "Scattering phase function for fibrous media," *International Journal of Heat and Mass Transfer*, vol. 33, no. 10, pp. 2183–2190, 1990.

Problems

13.1 The absorption coefficient of a liquid, confined between two parallel and transparent windows, is to be measured by the transmission method. The detector signals from transmission measurements with varying liquid thickness are to be used.

(*a*) Using transmission measurements for two thicknesses, show how the absorption coefficient κ may be deduced. Determine how errors in the transmissivity value and the liquid layer thickness affect the accuracy of κ.

(*b*) If transmission measurements are made for many thicknesses, can you devise a method that measures small absorption coefficients more accurately?

13.2 Show how the optical properties (n, k, and κ) of a semitransparent solid may be deduced from the three measurements taken with the apparatus of Myers and coworkers [58], as depicted in Fig. 13-11.